Figure 2

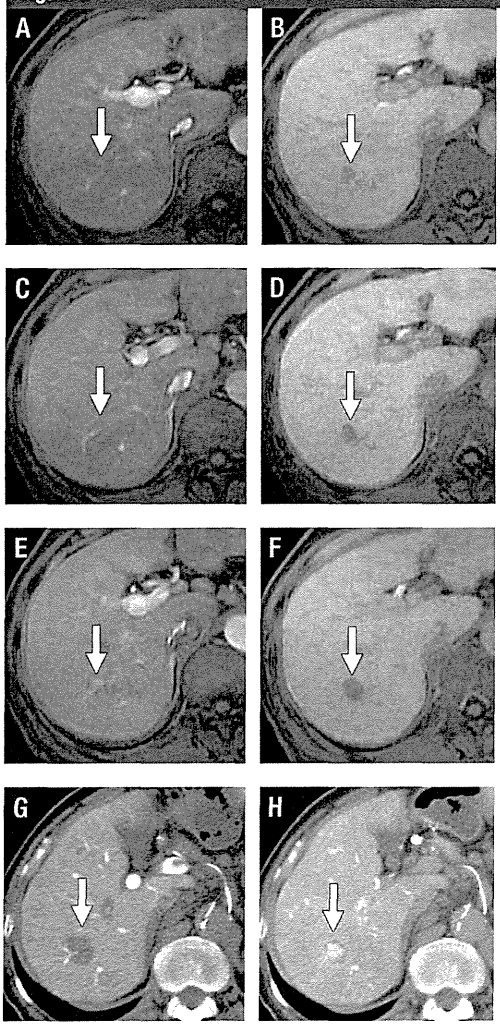

Figure 2: Growing hypovascular hepatic nodule (arrows) and subsequent hypervascularization in an 86-year-old man with hepatitis C and Child-Pugh class B cirrhosis. *A-F*, Axial gadoxetic acid–enhanced T1-weighted fat-suppressed three-dimensional gradient-recalled echo images obtained during (*A*, *C*, and *E*) arterial phase and (*B*, *D*, *F*) hepatobiliary phase obtained at (*A*, *B*) baseline, (*C*, *D*) day 94, and (*E*, *F*) day 176. At (*A*) baseline and (*C*) day 94, hepatic nodule in right posterior section showed neither arterial-phase enhancement nor portal-venous phase washout. Hepatobiliary phase images showed that maximum diameter increased from 8 mm at, *B*, baseline to 12 mm at, *D*, day 94, and TVDT was calculated as 170 days. *E*, Arterial-phase image at day 176 shows partial enhanceme of nodule. *G*, At day 194, CT arterial portographic image shows a well-defined, round perfusion defect and, *H*, CT hepatic arteriographic image shows marked enhancement corresponding to nodule. Nodule was diagnosed as HCC on the basis of image views and tumor markers.

Figure 3

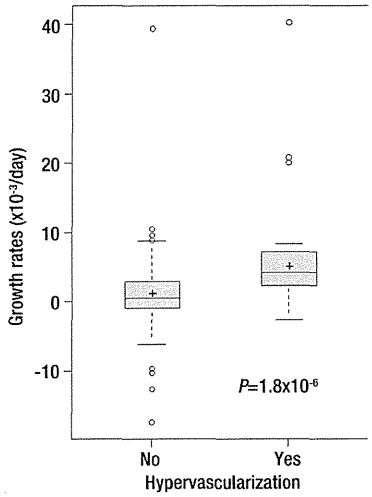

Figure 3: Box plot shows distribution of growth rates of 138 nodules. Median values and 25th and 75th percentiles are shown in each box plot. Vertical bars represent largest and smallest values that are not outliers. + = Mean; ○ = outlier of more than 1.5 times box length.

In comparison with hepatitis C infection or alcohol abuse, hepatitis B infection tends to induce macronodular (> 3 mm) cirrhosis (31). Thus, macronodular benign nodules in cases of hepatitis B cirrhosis might have been present in our subjects. Another possible reason why hepatitis B infection was a negative predictor for hypervascularization might be that antihepatitis B nucleoside analogs prevented the development of HCC (32).

The nodule-to-liver contrast ratios on unenhanced T1-weighted images and gadoxetic acid–enhanced hepatobiliary phase MR images were not a significant prognostic factor, which is consistent with previous reports (33). The signal intensity of nodules on T1-weighted images may be affected by intratumoral fat, metal, or glycogen in the surrounding hepatic parenchyma (1,34). The fat content of the nodules was also not a significant predictor of hypervascularization in our study. One possible reason for this was the fact that both early HCCs and dysplastic nodules could appear as intracellular lipid-containing lesions in cirrhotic livers (35). There was also no statistically significant association between initial diameter and hypervascularization in our study results. The probable reason for this was that most subjects (87%) had nodules of less than 15 mm in diameter (139 of 160 nodules).

The reported TVDT for HCC ranges from 18 to 605 days (1). The mean growth rate for HCCs smaller than 20 mm that showed no hyperintensity on T2-weighted MR images but that enhanced during arterial phase MR imaging was 10.5×10^{-3}/day (TVDT, 95 days; calculated by using data from Jeong et al [36]). The hypervascularization group, which was considered to be representative of an earlier stage of multistep carcinogenesis, showed the lower mean growth rate (6.5×10^{-3}/day [TVDT, 154

Figure 5

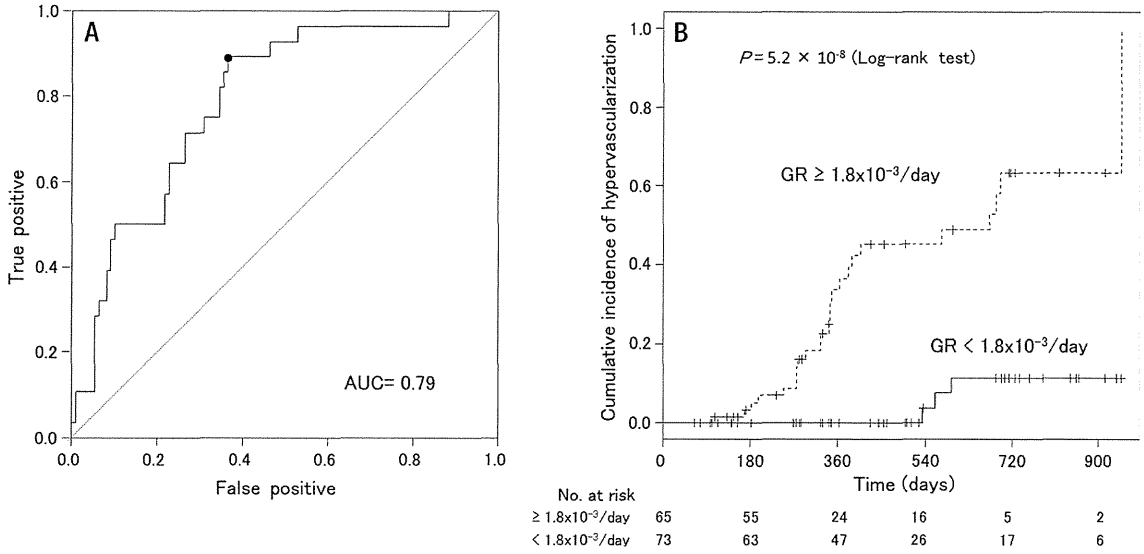

Figure 5: *A*, Graph shows receiver operating characteristic curve of growth rate *(GR)* for the prediction of hypervascularization (area under the curve *[AUC]*, 0.79). The optimal operating point on the receiver operating characteristic curve is marked with a black dot (growth rate, 1.8 × 10^{-3}/day). *B*, Kaplan-Meier analysis shows effect of growth rate on cumulative incidence of hypervascularization. Number of nodules at risk at each time point is shown at bottom of figure.

days]) than that reported in the Jeong et al study (36).

On the basis of these previous studies, hypovascular nodules larger than 15 mm are considered appropriate for biopsy. In cases with nodules less than 10 mm in diameter, the American Association for the Study of Liver Disease recommends imaging follow-up at 3–6 month intervals, with careful attention to increases in size or changes in vascular pattern. Repeated biopsy for nodules larger than 10 mm can be performed, but a needle liver biopsy has some disadvantages including inaccurate sampling caused by technical difficulties (eg, poor lesion or needle visualization, deeply located lesions, and hepatic fibrosis), risk of bleeding, and needle track seeding. Our growth analysis, along with baseline risk factors, might improve diagnostic discrimination with or without the need for biopsy, particularly for nodules measuring 10–15 mm. By using a cutoff growth rate of 1.8 × 10^{-3}/day (TVDT, 542 days), the calculated diameters at

Figure 4

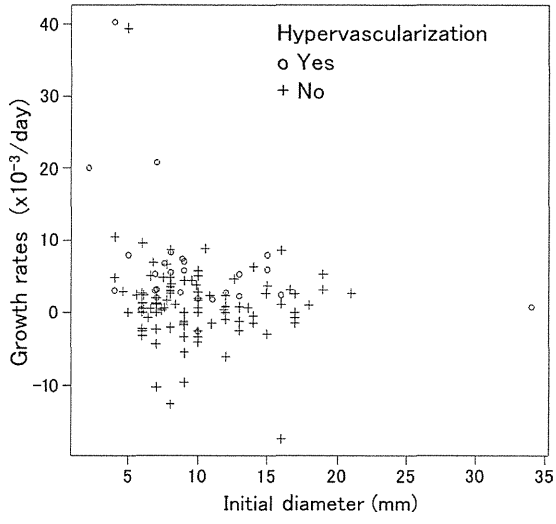

Figure 4: Scatterplot shows growth rate above the initial diameter. Individual nodules were coded according to whether they showed subsequent hypervascularization during the study period.

the 6-month follow-up examination for nodules with an initial diameter of 10, 11, 12, 13, and 14 mm were 10.8, 11.9, 13.0, 14.0, and 15.1 mm, respectively. We suggest that nodules with the risk factors for hypervascularization or those showing faster growth may justify more frequent follow-up or biopsy. If growth is slower, biopsy may not be needed, although the absence of growth does not rule out malignancy. According to expert opinion, nodules are declared benign only if they regress or remain stable for 2 years (37).

The reported incidence rates of hypervascularization vary throughout different studies. In our study, the overall 6- and 12-month cumulative percentages for hypervascularization were 10% and 25%, respectively, which is lower than the percentages calculated by Kumada et al (27.6% and 43.5%, respectively) (13). This may be partially explained by time frame, sample size, and/or follow-up policy of subjects in each study.

Our study had some limitations. It was a retrospective study, and this fact may have introduced bias in data homogeneity. To minimize sampling bias, we collected data from consecutive patients who underwent multiple gadoxetic acid–enhanced MR imaging examinations in two hospitals. Also, the duration of disease and date of diagnosis were potentially important confounders. However, they were not available for retrospective review.

Regarding the imaging technique, a relatively high rate (2 mL/sec) of injection of gadoxetic acid might reduce the performance of arterial-phase imaging. Some reports suggested that a lower injection rate might be appropriate owing to stretching the bolus without reducing the enhancement peak (38,39). However, we performed gadoxetic acid–enhanced MR imaging with optimized imaging technique (40) and timing (16) to acquire good images in the arterial phase.

On imaging analysis, our study was potentially limited by consensus review because we did not assess interobserver variability. Also, in the case of smaller nodules (< 10 mm), it might be difficult to obtain a clear correspondence between the MR images and those of the other modalities (CT, and in particular, contrast-enhanced US), even though well-trained radiologists and physicians reviewed the images.

Tumor growth kinetic calculations were based on the general assumption that tumor cells grow exponentially. This assumption might not hold true owing to fibrosis or to the intracellular lipid content of both the hepatic nodules and surrounding cirrhotic liver parenchyma. Because patients with Child-Pugh class C cirrhosis were excluded, the influence of fibrosis of the surrounding parenchyma is limited. Also, measurement errors associated with manual evaluation may have led to bias. However, to improve accuracy all measurements were performed in the same manner, by using T1-weighted three-dimensional gradient-echo images that provided high spatial resolution (7). A large-scale prospective validation study is necessary to confirm our proposed cutoff values.

In conclusion, hypervascularization occurs in about one-third of the hypovascular nodules that show hypointensity on gadoxetic acid–enhanced hepatobiliary phase MR images. MR imaging findings, including hyperintensity on T2-weighted images and a higher growth rate, may predict arterial hypervascularization, which may lead to early diagnosis and treatment of HCC.

Disclosures of Conflicts of Interest: T.H. Financial activities related to the present article: Received Osaka Cancer Foundation grant in 2010. Financial activities not related to the present article: none to disclose. Other relationships: none to disclose. **T. Murakami** No relevant conflicts of interest to disclose. **Y.I.** No relevant conflicts of interest to disclose. **M.O.** No relevant conflicts of interest to disclose. **M.H.** No relevant conflicts of interest to disclose. **Y.K.** No relevant conflicts of interest to disclose. **S. Kogita** No relevant conflicts of interest to disclose. **S. Kumano** No relevant conflicts of interest to disclose. **M.K.** No relevant conflicts of interest to disclose. **T. Mochizuki** No relevant conflicts of interest to disclose.

References

1. Willatt JM, Hussain HK, Adusumilli S, Marrero JA. MR Imaging of hepatocellular carcinoma in the cirrhotic liver: challenges and controversies. Radiology 2008;247(2):311–330.
2. Bruix J, Sherman M; American Association for the Study of Liver Diseases. Management of hepatocellular carcinoma: an update. Hepatology 2011;53(3):1020–1022.
3. Giovagnoni A, Paci E. Liver. III: Gadolinium-based hepatobiliary contrast agents (Gd-EOB-DTPA and Gd-BOPTA/Dimeg). Magn Reson Imaging Clin N Am 1996;4(1):61–72.
4. Bluemke DA, Sahani D, Amendola M, et al. Efficacy and safety of MR imaging with liver-specific contrast agent: U.S. multicenter phase III study. Radiology 2005;237(1):89–98.
5. Haradome H, Grazioli L, Tinti R, et al. Additional value of gadoxetic acid-DTPA-enhanced hepatobiliary phase MR imaging in the diagnosis of early-stage hepatocellular carcinoma: comparison with dynamic triple-phase multidetector CT imaging. J Magn Reson Imaging 2011;34(1):69–78.
6. Okada M, Imai Y, Kim T, et al. Comparison of enhancement patterns of histologically confirmed hepatocellular carcinoma between gadoxetate- and ferucarbotran-enhanced magnetic resonance imaging. J Magn Reson Imaging 2010;32(4):903–913.
7. Lee VS, Lavelle MT, Rofsky NM, et al. Hepatic MR imaging with a dynamic contrast-enhanced isotropic volumetric interpolated breath-hold examination: feasibility, reproducibility, and technical quality. Radiology 2000;215(2):365–372.
8. Golfieri R, Renzulli M, Lucidi V, Corcioni B, Trevisani F, Bolondi L. Contribution of the hepatobiliary phase of Gd-EOB-DTPA-enhanced MRI to Dynamic MRI in the detection of hypovascular small (≤ 2 cm) HCC in cirrhosis. Eur Radiol 2011;21(6):1233–1242.
9. International Consensus Group for Hepatocellular NeoplasiaThe International Consensus Group for Hepatocellular Neoplasia. Pathologic diagnosis of early hepatocellular carcinoma: a report of the international consensus group for hepatocellular neoplasia. Hepatology 2009;49(2):658–664.
10. Hayashi M, Matsui O, Ueda K, et al. Correlation between the blood supply and grade of malignancy of hepatocellular nodules associated with liver cirrhosis: evaluation by CT during intraarterial injection of contrast medium. AJR Am J Roentgenol 1999;172(4):969–976.
11. Yu JS, Chung JJ, Kim JH, Kim KW. Fat-containing nodules in the cirrhotic liver: chemical shift MRI features and clinical implications. AJR Am J Roentgenol 2007;188(4):1009–1016.
12. Motosugi U, Ichikawa T, Sano K, et al. Outcome of hypovascular hepatic nodules revealing no gadoxetic acid uptake in patients

with chronic liver disease. J Magn Reson Imaging 2011;34(1):88–94.

13. Kumada T, Toyoda H, Tada T, et al. Evolution of hypointense hepatocellular nodules observed only in the hepatobiliary phase of gadoxetate disodium-enhanced MRI. AJR Am J Roentgenol 2011;197(1):58–63.
14. Sakamoto M, Hirohashi S, Shimosato Y. Early stages of multistep hepatocarcinogenesis: adenomatous hyperplasia and early hepatocellular carcinoma. Hum Pathol 1991;22(2):172–178.
15. Makuuchi M, Kokudo N, Arii S, et al. Development of evidence-based clinical guidelines for the diagnosis and treatment of hepatocellular carcinoma in Japan. Hepatol Res 2008;38(1):37–51.
16. Kagawa Y, Okada M, Kumano S, et al. Optimal scanning protocol of arterial dominant phase for hypervascular hepatocellular carcinoma with gadolinium-ethoxybenzyl-diethylenetriamine pentaacetic acid-enhanced MR. J Magn Reson Imaging 2011;33(4):864–872.
17. Goshima S, Kanematsu M, Kondo H, et al. MDCT of the liver and hypervascular hepatocellular carcinomas: optimizing scan delays for bolus-tracking techniques of hepatic arterial and portal venous phases. AJR Am J Roentgenol 2006;187(1):W25–W32.
18. Hori M, Murakami T, Kim T, Nakamura H. Diagnosis of hepatic neoplasms using CT arterial portography and CT hepatic arteriography. Tech Vasc Interv Radiol 2002; 5(3):164–169.
19. Kudo M, Hatanaka K, Maekawa K. Newly developed novel ultrasound technique, defect reperfusion ultrasound imaging, using sonazoid in the management of hepatocellular carcinoma. Oncology 2010;78(Suppl 1):40–45.
20. Collins VP, Loeffler RK, Tivey H. Observations on growth rates of human tumors. Am J Roentgenol Radium Ther Nucl Med 1956;76(5):988–1000.
21. Schwartz M. A biomathematical approach to clinical tumor growth. Cancer 1961; 14:1272–1294.
22. R Development Core Team. R: A language and environment for statistical computing. Vienna, Austria: R Foundation for Statistical Computing, 2010.
23. Lin DY. Cox regression analysis of multivariate failure time data: the marginal approach. Stat Med 1994;13(21):2233–2247.
24. Fawcett T. An introduction to ROC analysis. Pattern Recognit Lett 2006;27(8):861–874.
25. Kadoya M, Matsui O, Takashima T, Nonomura A. Hepatocellular carcinoma: correlation of MR imaging and histopathologic findings. Radiology 1992;183(3):819–825.
26. Ohtomo K, Baron RL, Dodd GD 3rd, Federle MP, Ohtomo Y, Confer SR. Confluent hepatic fibrosis in advanced cirrhosis: evaluation with MR imaging. Radiology 1993;189(3):871–874.
27. Kim T, Baron RL, Nalesnik MA. Infarcted regenerative nodules in cirrhosis: CT and MR imaging findings with pathologic correlation. AJR Am J Roentgenol 2000;175(4): 1121–1125.
28. Hussain HK, Syed I, Nghiem HV, et al. T2-weighted MR imaging in the assessment of cirrhotic liver. Radiology 2004;230(3): 637–644.
29. Fattovich G, Stroffolini T, Zagni I, Donato F. Hepatocellular carcinoma in cirrhosis: incidence and risk factors. Gastroenterology 2004;127(5,Suppl 1):S35–S50.
30. Bolondi L, Sofia S, Siringo S, et al. Surveillance programme of cirrhotic patients for early diagnosis and treatment of hepatocellular carcinoma: a cost effectiveness analysis. Gut 2001;48(2):251–259.
31. Rozario R, Ramakrishna B. Histopathological study of chronic hepatitis B and C: a comparison of two scoring systems. J Hepatol 2003;38(2):223–229.
32. Matsumoto A, Tanaka E, Rokuhara A, et al. Efficacy of lamivudine for preventing hepatocellular carcinoma in chronic hepatitis B: A multicenter retrospective study of 2795 patients. Hepatol Res 2005;32(3): 173–184.
33. Kobayashi S, Matsui O, Gabata T, et al. Gadolinium ethoxybenzyl diethylenetriamine pentaacetic Acid-enhanced magnetic resonance imaging findings of borderline lesions at high risk for progression to hypervascular classic hepatocellular carcinoma. J Comput Assist Tomogr 2011;35(2): 181–186.
34. Ebara M, Fukuda H, Kojima Y, et al. Small hepatocellular carcinoma: relationship of signal intensity to histopathologic findings and metal content of the tumor and surrounding hepatic parenchyma. Radiology 1999; 210(1):81–88.
35. Basaran C, Karcaaltincaba M, Akata D, et al. Fat-containing lesions of the liver: cross-sectional imaging findings with emphasis on MRI. AJR Am J Roentgenol 2005; 184(4):1103–1110.
36. Jeong YY, Mitchell DG, Kamishima T. Small (<20 mm) enhancing hepatic nodules seen on arterial phase MR imaging of the cirrhotic liver: clinical implications. AJR Am J Roentgenol 2002;178(6):1327–1334.
37. Bruix J, Sherman M; Practice Guidelines Committee, American Association for the Study of Liver Diseases. Management of hepatocellular carcinoma. Hepatology 2005;42(5):1208–1236.
38. Zech CJ, Vos B, Nordell A, et al. Vascular enhancement in early dynamic liver MR imaging in an animal model: comparison of two injection regimen and two different doses Gd-EOB-DTPA (gadoxetic acid) with standard Gd-DTPA. Invest Radiol 2009;44(6):305–310.
39. Chung SH, Kim MJ, Choi JY, Hong HS. Comparison of two different injection rates of gadoxetic acid for arterial phase MRI of the liver. J Magn Reson Imaging 2010;31(2):365–372.
40. Kim KA, Herigault G, Kim MJ, Chung YE, Hong HS, Choi SY. Three-dimensional contrast-enhanced hepatic MR imaging: comparison between a centric technique and a linear approach with partial Fourier along both slice and phase directions. J Magn Reson Imaging 2011;33(1):160–166.

Liver INTERNATIONAL
OFFICIAL JOURNAL OF THE INTERNATIONAL ASSOCIATION FOR THE STUDY OF THE LIVER

Liver International ISSN 1478-3223

BASIC STUDIES

A glycyrrhizin-containing preparation reduces hepatic steatosis induced by hepatitis C virus protein and iron in mice

Masaaki Korenaga[1], Isao Hidaka[2], Sohji Nishina[1], Aya Sakai[3], Akane Shinozaki[3], Toshikazu Gondo[4], Takakazu Furutani[5], Hiroo Kawano[6], Isao Sakaida[2] and Keisuke Hino[1]

1 Department of Hepatology and Pancreatology, Kawasaki Medical University, Okayama, Japan
2 Department of Gastroenterology and Hepatology, Yamaguchi University Graduate School of Medicine, Yamaguchi, Japan
3 Department of Basic Laboratory Sciences, Yamaguchi University Graduate School of Medicine, Yamaguchi, Japan
4 Department of Surgical Pathology, Yamaguchi University Hospital, Yamaguchi, Japan
5 Department of Gastroenterology and Hepatology, Shuto General Hospital, Yamaguchi, Japan
6 Department of Pathology, Yamaguchi University Graduate School of Medicine, Yamaguchi, Japan

Keywords
carnitine palmitoyl transferase – mitochondria – oxidative stress – reactive oxygen species – transgenic mice

Abbreviations
ALT, alanine aminotransferase; ATF6, activating transcription factor 6; CCl_4, carbon tetrachloride; CHOP, CCAAT/enhancer-binding protein homology protein; CPT, carnitine palmitoyl transferase; ER, endoplasmic reticulum; FAS, fatty acid synthetase; γ-GCS, γ-glutamylcysteine synthetase; GSH, reduced glutathione; HCC, hepatocellular carcinoma; HCV, hepatitis C virus; IRE1, inositol-requiring enzyme 1; NAC, *N*-acetyl cysteine; PERK, PKR-like ER kinase; p-eIF2α, phosphorylated eukaryotic initiation factor-2α; PKR, RNA-activated protein kinase; ROS, reactive oxygen species; RT-PCR, reverse-transcription polymerase chain reaction; SNMC, Stronger Neo-Minophagen C; SREBP1, sterol regulatory element-binding protein 1; XBP-1, X-box DNA-binding protein 1.

Correspondence
Keisuke Hino, MD, PhD, Department of Hepatology and Pancreatology, Kawasaki Medical University, 577 Matsushima, Kurashiki, Okayama 701-0192, Japan
Tel: +81-86-4621111
Fax: +81-86-4641196
e-mail: khino@med.kawasaki-m.ac.jp

Received 1 July 2010
Accepted 7 January 2011

DOI:10.1111/j.1478-3231.2011.02469.x

Abstract

Background/Aim: A European randomized trial showed biochemical effects of 6-month treatment with Stronger Neo-Minophagen C™ (SNMC), a glycyrrhizin-containing preparation, in patients with chronic hepatitis C, but its underlying mechanisms remain elusive. We reported previously that SNMC exhibits an anti-oxidative effect in hepatitis C virus (HCV) transgenic mice that develop marked hepatic steatosis with mitochondrial injury under iron overloading. Hepatic steatosis and iron overload are oxidative stress-associated pathophysiological features in chronic hepatitis C. The aim of this study was to investigate whether long-term treatment with SNMC could prevent the development of hepatic steatosis in iron-overloaded HCV transgenic mice. *Methods:* C57BL/6 transgenic mice expressing the HCV polyprotein were fed an excess iron diet concomitantly with intraperitoneal injection of saline, SNMC, or seven-fold-concentrated SNMC thrice weekly for 6 months. *Results:* Stronger Neo-Minophagen C™ inhibited the development of hepatic steatosis in a dose-dependent manner without affecting hepatic iron content, attenuated ultrastructural alterations of mitochondria of the liver, activated mitochondrial β-oxidation with increased expression of carnitine palmitoyl transferase I and decreased the production of reactive oxygen species in the liver in iron-overloaded transgenic mice. However, SNMC hardly affected the unfolded protein response, which post-transcriptionally activates sterol regulatory element-binding protein 1, a transcription factor involved in lipid synthesis, even though we reported previously the activation of the unfolded protein response in the same iron-overloaded transgenic mice. *Conclusions:* These results suggest that SNMC prevents hepatic steatosis possibly by protecting mitochondria against oxidative stress induced by HCV proteins and iron overload.

Hepatitis C virus (HCV) causes acute and chronic hepatitis, cirrhosis and hepatocellular carcinoma (HCC) (1). Because current antiviral treatment can only eliminate the virus in approximately 50% of patients (2), therapies to reduce disease progression in chronically infected individuals would be of great benefit. In Japan, Stronger Neo-Minophagen C™ (SNMC), a glycyrrhizin-containing preparation, has been used as a treatment for

chronic hepatitis for more than 30 years. SNMC contained glycyrrhizin as the main active ingredient at first, and later a change was made in its composition on the basis of pharmacological studies including animal experiments and clinical studies. Currently, it is available in an injectable form for intravenous administration, containing 0.2% glycyrrhizin, 0.1% L-cystein and 2.0% glycine in physiological solution. A recent European randomized trial showed biochemical effects of 26-week treatment with SNMC in patients with chronic hepatitis C (3). In addition, Arase *et al.* (4) demonstrated that long-term usage of SNMC was effective in preventing HCC development in Japanese patients with chronic hepatitis C. However, the mechanisms by which SNMC prevents disease progression of chronic hepatitis C remain elusive.

Oxidative stress has been proposed to be one of the mechanisms of liver injury in HCV-associated chronic liver diseases (5), and hepatic steatosis and/or mitochondrial injury are well-known features in chronic hepatitis C (6, 7). We reported that HCV transgenic mice fed an excess iron diet show marked steatosis and mitochondrial injury at 6 months, and an increase in the hepatic lipid peroxidation products and the subsequent development of HCC at 12 months after the initiation of feeding (8). We also showed that a single injection of SNMC protected hepatocytes against carbon tetrachloride (CCl_4)-induced oxidative stress and mitochondrial injury in these transgenic mice without iron overload (9). These results prompted us to investigate whether SNMC inhibited the development of hepatic steatosis in terms of prevention of disease progression in chronic hepatitis C. The aim of this study was to examine whether long-term treatment with SNMC could prevent the development of hepatic steatosis in HCV transgenic mice fed an excess iron diet. In the present study, we show that SNMC reduces hepatic steatosis induced by HCV protein and iron overload in mice by means of a protective effect against mitochondrial injury.

Materials and methods

Animals and experimental design

The transgene pAlbSVPA-HCV, containing the full-length polyprotein-coding region under the control of the murine albumin promoter/enhancer, was described in detail (10, 11). Of the four transgenic lineages with evidence of RNA transcription of the full-length HCV-N open reading frame (FL-N), the FL-N/35 lineage proved capable of breeding in large numbers. There is no inflammation in the transgenic liver (11). Male FL-N/35 transgenic mice were fed an excess iron diet (carbonyl iron 225 mg/kg diet) at the age of 8 weeks, injected intraperitoneally with 50 µl of saline (control), SNMC or seven-fold-concentrated SNMC (supplied by Minophagen Pharmaceutical Co. Ltd, Tokyo, Japan) three times weekly and killed by intraperitoneal injection of 10% pentbarbital sodium preceded by 12-h fasting at 6 months after initiation of feeding according to the criteria outlined in the Guide for the Care and Use of Laboratory Animals.

Histological procedures

A portion of liver tissue was immediately snap frozen in liquid nitrogen for RNA extraction, protein extraction and determination of hepatic triglyceride and iron concentrations. The remaining liver tissue was fixed in 4% paraformaldehyde in phosphate-buffered saline and embedded in paraffin for histological analysis. Liver sections were stained with haematoxylin and eosin and Masson's trichrome method for fibrosis.

Hepatic triglyceride content

Lipids were extracted from the homogenized liver tissue by the method of Bligh and Dyer (12). The triglyceride levels were measured with a TGE test Wako kit (Wako Pure Chemicals, Tokyo, Japan), according to the manufacturer's instructions. Protein concentrations in liver were determined by the method of Lowry *et al.* (13), using a DC protein assay kit (Bio-Rad Laboratories, Hercules, CA, USA).

Hepatic iron concentration and hepcidin mRNA

The iron concentration in the liver was measured by atomic absorption spectrometry (Hitachi Z-6100, Tokyo, Japan), as described previously (8), and expressed as micrograms Fe/g of tissue (wet weight). One-step real-time reverse-transcription polymerase chain reaction was also performed as described previously (8). The primers amplifying the genes coding hepcidin and β-actin were as follows: hepcidin, sense; TCCTGCTTCTCCTCCTTGCC, antisense; GTCTGCCCTGCTTTCTTCCC (GenBank accession number, NM_032541) and β-actin, sense; TGACAGGATGCAGAAGGAGA, antisense; GCTGGAA GGTGGACAGTGAG (GenBank accession number, NM_ 007393).

Immunoblotting

Lysates of liver were separated by sodium dodecyl sulphate–polyacrylamide gel electrophoresis. The proteins were transferred to polyvinylidene difluoride membranes (Millipore, Bedford, MA, USA), blocked overnight at 4 °C with 5% skim milk and 0.1% Tween 20 in Tris-buffered saline, and subsequently incubated for 1 h at room temperature with an anti-rabbit carnitine palmitoyl transferase I (CPTI) antibody, anti-rabbit CPTII antibody (Alpha Diagnostic International, San Antonio, TX, USA), anti-rabbit sterol regulatory element-binding protein 1 (SREBP1) antibody (Santa Cruz Biotechnology Inc., Santa Cruz, CA, USA), anti-rabbit fatty acid synthetase (FAS) antibody (Cell Signaling Technology Inc., Boston, MA, USA), anti-mouse X-box

DNA-binding protein 1 (XBP-1) antibody (Santa Cruz Biotechnology Inc.) or anti-bacterially expressed, mouse CCAAT/enhancer-binding protein homology protein (CHOP) fusion protein antibody (Abcam, Cambridge, UK). Exceptionally, the proteins were blocked for 1 h at room temperature and subsequently incubated overnight at 4 °C with an anti-rabbit phosphorylated eukaryotic initiation factor-2α (p-eIF2α) antibody (Cell Signaling Technology Inc.).

Electron microscopy

Liver specimens were fixed in 2.1% glutaraldehyde, post-fixed in 1% osmium tetroxide, dehydrated in graded ethanol and propylene dioxide and embedded in Epok. Thick sections (1 μm in width) were stained with toluidine blue to identify steatosis by light microscopy. Thin sections were stained with uranyl acetate and lead citrate, and examined using a Hitachi-7000 transmission electron microscope (Hitachi Ltd., Tokyo, Japan). The length of mitochondria was measured using IMAGE-PRO PLUS 4.0 software (Media Cybernetics Inc., Bethesda, MD, USA) for two randomly selected areas of electron microscopic images in each mice to quantify ultrastructural alterations of mitochondria.

In vivo formation of [^{14}C]CO_2 from [U-^{14}C] palmitic acid

A tracer dose of [U-^{14}C] palmitic acid (150 μCi/kg; 0.16 μmol/kg, American Biosciences, St Louis, MO, USA) was administered by gastric intubation in 0.2 ml of corn oil, preceded by fasting for 42 h, as described previously (8). The animal was then placed for 6 h in a small plastic cage swept by an airflow of 50 ml/min. The outflow was bubbled into 30 ml of monoethanolamine. After 6 h, 1 ml was removed and counted for [^{14}C] CO_2 activity with an Aloka Liquid Scintillation Counter 5100 (Aloka Co. Ltd., Tokyo, Japan).

In situ detection of reactive oxygen species

In situ reactive oxygen species (ROS) production in the liver was assessed by staining with dihydroethidium as described previously (14). In the presence of ROS, dihydroethidium (Invitrogen Corp., Carlsbad, CA, USA) is oxidized to ethidium bromide and stains nuclei bright red by intercalating with the DNA (15). Fluorescence intensity was quantified using NIH image analysis software for three randomly selected areas of digital images for each mouse.

Statistical analysis

Quantitative values are expressed as mean ± SD. Two groups among multiple groups were compared by the rank-based, Kruskal–Wallis ANOVA test followed by the Scheffé test. Data between two groups were compared by Student's *t*-test. A P value of < 0.05 was considered to be significant.

Results

Serum alanine aminotransferase levels and hepatic triglyceride accumulation

Six-month treatment with SNMC or seven-fold-concentrated SNMC significantly reduced serum alanine aminotransferase (ALT) ($P < 0.05$) in FL-N/35 transgenic mice fed the excess iron diet (Fig. 1A). Transgenic mice fed the excess iron diet developed severe steatosis including the centrilobular microvesicular type, as described previously (8, 16). SNMC reduced hepatic triglyceride content in a dose-dependent manner ($P < 0.05$, $P < 0.01$, Fig. 1B). SNMC obviously reduced the centrilobular microvesicular steatosis and moderately decreased hepatic steatosis in the remaining areas of hepatic lobules, whereas seven-fold-concentrated SNMC almost completely suppressed hepatic steatosis (Fig. 1C). Mice in the three groups (control, SNMC and seven-fold-concentrated SNMC) showed no evidence of intrahepatic inflammation or fibrosis.

Hepatic iron content

We reported that iron overload reinforced hepatic steatosis in FL-N/35 transgenic mice (8). We first measured hepatic iron levels and the expression of hepcidin, a negative regulator in iron homeostasis, to assess whether SNMC attenuated hepatic iron overload. As shown in Figure 2, 6-month treatment with SNMC or seven-fold-concentrated SNMC changed neither the hepatic iron level nor the hepcidin expression in transgenic mice fed the excess iron diet, suggesting that SNMC inhibited hepatic steatosis without affecting iron overload.

Mitochondrial ultrastructure

As we observed previously the attenuation of CCl_4-induced ultrastructural alterations of mitochondria by SNMC in FL-N/35 transgenic mice (9), and found obvious reduction of centrilobular microvesicular steatosis by SNMC in the present study, we next examined the ultrastructure of the hepatic mitochondria in FL-N/35 transgenic mice fed the excess iron diet. Ultrastructural alterations such as irregularly sized mitochondria, swollen mitochondria or disorganized cristae that were observed in FL-N/35 transgenic mice fed the excess iron were much less frequently found after the 6-month treatment with SNMC in a dose-dependent manner (Fig. 3A–C). The mean length of mitochondria was significantly greater in mice without SNMC than in those with SNMC (Fig. 3D). Thus, SNMC attenuated ultrastructural alterations of mitochondria of the liver in FL-N/35 transgenic mice fed the excess iron diet.

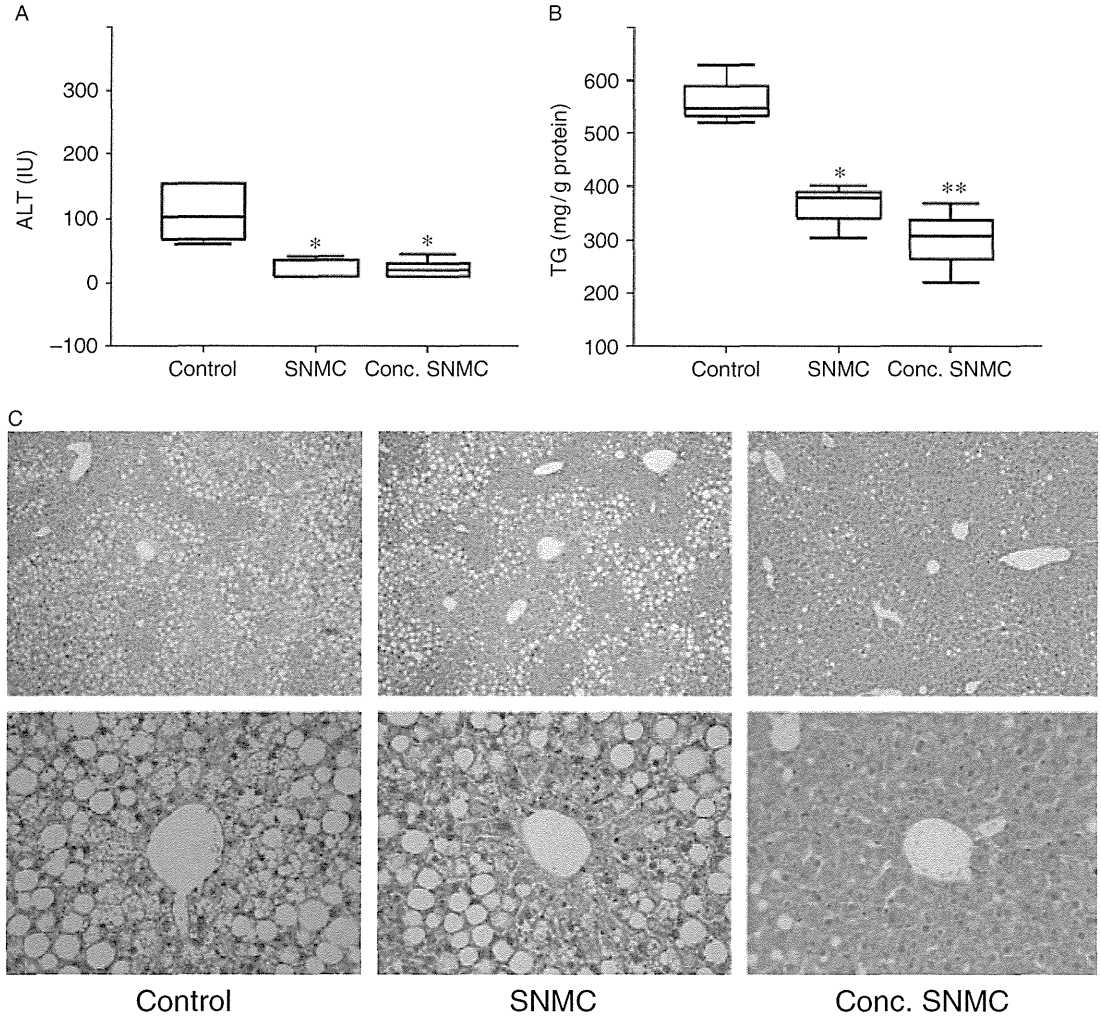

Fig. 1. Serum alanine aminotransferase (ALT) levels, hepatic triglyceride levels and hepatic steatosis in iron-overloaded FL-N/35 transgenic mice in three groups. (A) Serum ALT levels in six mice in each group. (B) Hepatic triglyceride levels in three mice in each group. ALT and triglyceride levels are shown as box plot profiles. The bottom and top edges of the boxes are the 25th and 75th percentiles respectively. The median value is shown by the line within the box. (C) Hepatic steatosis in mice in each group (haematoxylin and eosin, original magnification × 100 for upper panel and × 400 for lower panel). Control, transgenic mice injected intraperitoneally with 50 μl of saline three times weekly for 6 months; Stronger Neo-Minophagen C^{TM} (SNMC), transgenic mice injected intraperitoneally with 50 μl of SNMC three times weekly for 6 months; Conc. SNMC, transgenic mice injected intraperitoneally with 50 μl of seven-fold-concentrated SNMC three times weekly for 6 months. *$P < 0.05$, $P < 0.01$ vs control.

Degradation activity of fatty acid

We next examined *in vivo* formation of [^{14}C]CO_2 from [U-^{14}C] palmitic acid (C16:0) to assess whether SNMC improved mitochondrial function. Palmitic acid is a long-chain fatty acid. Mitochondria catalyse the β-oxidation of the bulk of short-, medium- and long-chain fatty acids (17). As shown in Figure 4A, SNMC significantly increased the *in vivo* formation of [^{14}C]CO_2 from [U-^{14}C] palmitic acid in FL-N/35 transgenic mice fed the excess iron diet ($P < 0.05$). These results suggested that SNMC improved mitochondrial β-oxidation activity.

Carnitine palmitoyl transferase I expression

Carnitine palmitoyl transferase I and CPTII regulate oxidation of long-chain fatty acids in the mitochondria. CPTI, a transmembrane enzyme of the mitochondrial outer membrane, has been shown to be the rate-limiting step in the β-oxidation of long-chain fatty acids (18). The expression of CPTI, but not CPTII, significantly increased after the 6-month treatment with SNMC or seven-fold-concentrated SNMC ($P < 0.005$, Fig. 4B). We reported previously the decreased expression of CPTI in FL-N/35 transgenic mice fed the excess iron diet as compared with nontransgenic mice fed the control diet

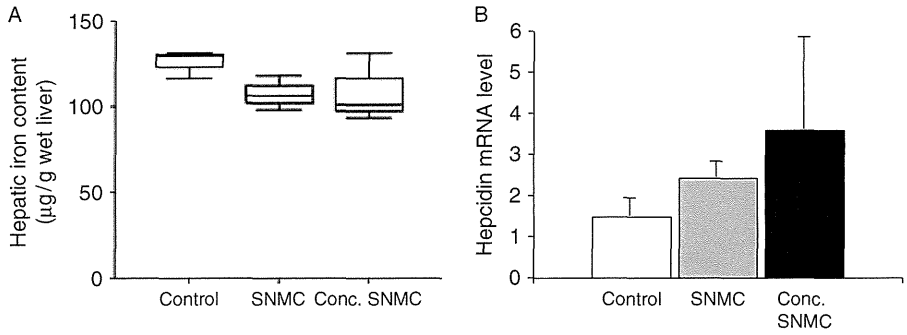

Fig. 2. Iron content and hepcidin mRNA expression in the liver in iron-overloaded FL-N/35 transgenic mice in each group. (A) Hepatic iron concentrations were measured by atomic absorption spectrometry in three mice in each group. The results are shown as box plot profiles. The bottom and top edges of the boxes are the 25th and 75th percentiles respectively. The median value is shown by the line within the box. (B) The expression levels of hepcidin mRNA was measured by reverse-transcription polymerase chain reaction in three mice in each group. The relative quantities of hepcidin mRNA were normalized to β-actin mRNA. Control, Stronger Neo-Minophagen C^{TM} (SNMC) and Conc. SNMC; see legend for Figure 1.

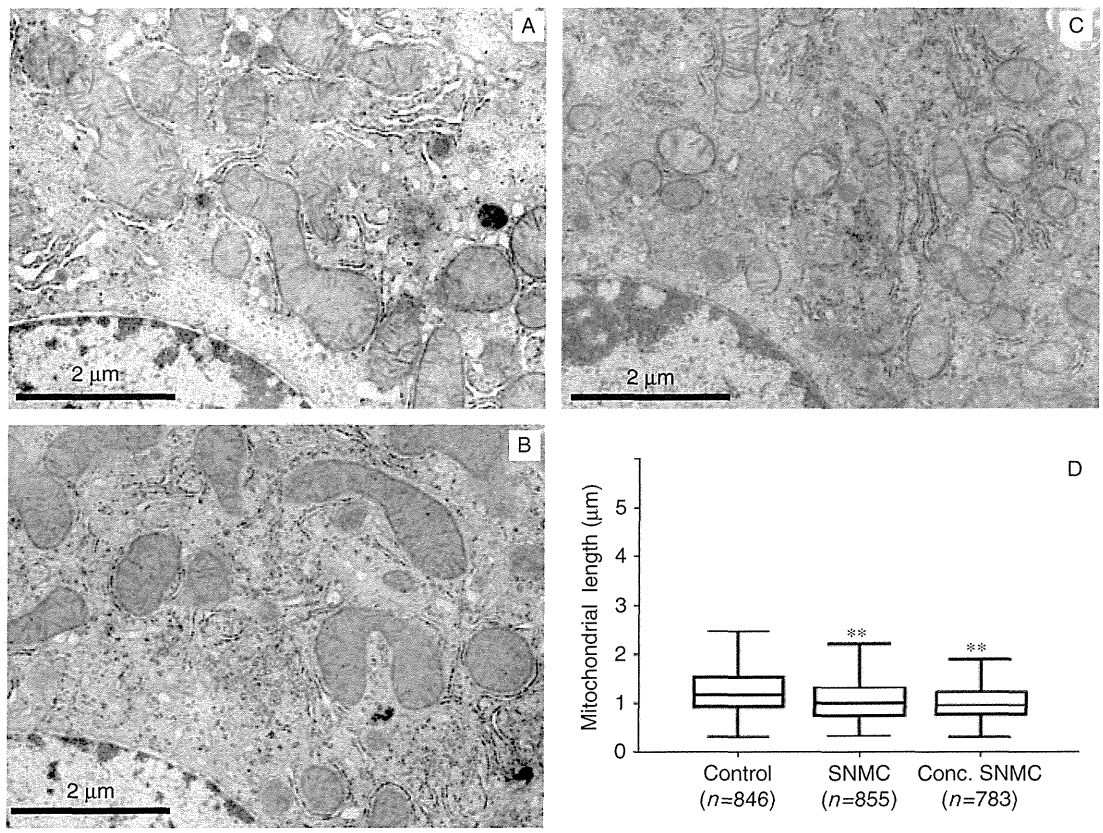

Fig. 3. Electron microscopy of the liver of an iron-overloaded FL-N/35 transgenic mouse from each group. Ultrastructural alterations such as irregularly sized mitochondria, swollen mitochondria and disorganized cristae that were observed in the iron-overloaded FL-N/35 transgenic mouse were much less frequently found after a 6-month treatment with Stronger Neo-Minophagen C^{TM} (SNMC) in a dose-dependent manner. The magnification scale is indicated in the left-lower corner of each picture. The length of mitochondria was assessed for three mice in each group and measured using IMAGE-PRO PLUS 4.0 software for two randomly selected areas of electron microscopic images in each mice. The numbers in parentheses represent the total number of mitochondria examined in each group. Control, SNMC and Conc. SNMC; see legend for Figure 1. (A) Control; (B) SNMC; (C) Conc. SNMC; and (D) the length of mitochondria. $^{**}P < 0.0001$ vs control.

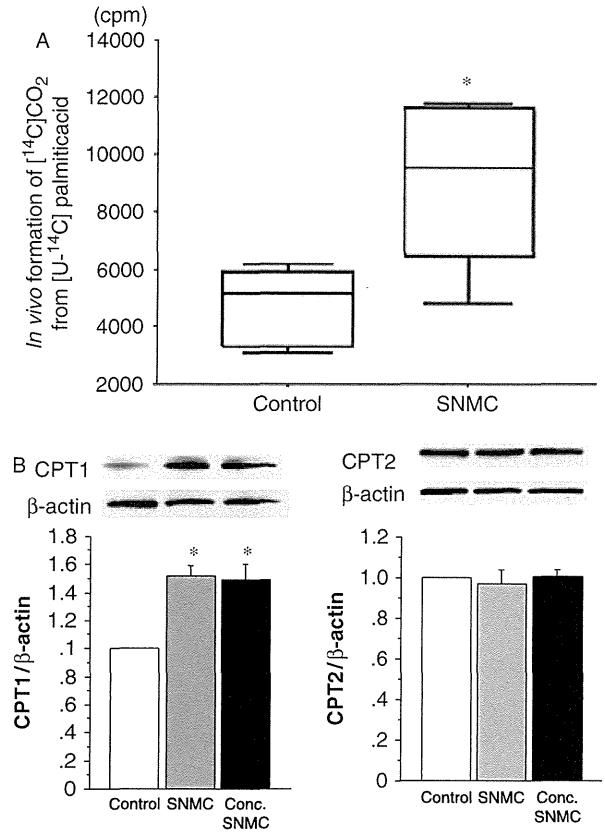

Fig. 4. *In vivo* formation of [^{14}C]CO_2 from [U-^{14}C] palmitic acid and hepatic expression of carnitine palmitoyl transferase I (CPTI) and CPTII in iron-overloaded FL-N/35 transgenic mice in each group. (A) A tracer dose of [U-^{14}C] palmitic acid (150 μCi/kg; 0.16 μmol/kg) was administered by gastric intubation in 0.2 ml of corn oil, preceded by fasting for 42 h. The animal was then placed for 6 h in a small plastic cage swept by an airflow of 50 ml/min. The outflow was bubbled into 30 ml of monoethanolamine. After 6 h, 1 ml was removed and counted for [^{14}C] CO_2 activity. This experiment was carried out for five mice in each group. The results are shown as box plot profiles. The bottom and top edges of the boxes are the 25th and 75th percentiles respectively. The median value is shown by the line within the box. (B) Immunoblots for CPTI and CPTII were performed using liver lysates from four mice in each group. The degree of protein expression was normalized with β-actin. Control, Stronger Neo-Minophagen C^{TM} (SNMC) and Conc. SNMC; see legend for Figure 1. *$P < 0.05$ vs control.

(16), which may be related to the association of HCV core protein with the mitochondrial outer membrane (19). Together with improvement of the mitochondrial structure, β-oxidation activity and CPTI expression, SNMC had a protective effect against mitochondrial injury induced by HCV proteins and iron overload.

Reactive oxygen species production

We have reported previously that HCV core protein increases ROS production through inhibition of mitochondrial electron transport (19), and found increased ROS production in FL-N/35 transgenic mice fed the excess iron diet as compared with nontransgenic mice fed the control diet (16). Therefore, we evaluated *in situ* ROS production to assess whether SNMC reduces ROS production in the liver in terms of a protective effect against mitochondrial injury. ROS production was significantly reduced by SNMC in a dose-dependent manner ($P < 0.005$, $P < 0.001$, Fig. 5). Thus, SNMC reduced hepatic steatosis by protecting mitochondria against oxidative stress induced by HCV proteins and iron overload.

Unfolded protein response and sterol regulatory element-binding protein 1 expression

We next evaluated the effect of SNMC on the unfolded protein response and the expression of SREBP1, a transcription factor that activates genes required for lipogenesis (20), because we found in our previous study that not only the decreased CPTI expression but also the increased SREBP1 expression owing to the activated unfolded protein response contributed to the development of hepatic steatosis in FL-N/35 transgenic mice fed the excess iron diet (16). The unfolded protein response signalling cascades are initiated by three endoplasmic reticulum (ER)-resident sensors: inositol-requiring enzyme 1 (IRE1), RNA-activated protein kinase-like ER kinase (PERK) and activating transcription factor 6 (ATF6) (21). IRE1 activation splices unspliced XBP-1 (uXBP-1) to form spliced XBP-1 (sXBP-1) mRNA (22), and was assessed by the sXBP-1 protein level (23). PERK activation was evaluated by measurement of p-eIF2α and CHOP (24). ATF6 activation was assessed by uXBP-1 expression (25). Six-month treatment with SNMC or seven-fold-concentrated SNMC did not change the expression of sXBP-1, CHOP, SREBP1 or FAS, a target gene of SREBP1, but decreased the expression of uXBP-1 and p-eIF2α (Fig. 6). These results suggested that SNMC inhibited hepatic steatosis through a protective effect against mitochondrial injury rather than restoration of activated lipogenesis in FL-N/35 transgenic mice fed the excess iron diet, even though it may attenuate the unfolded protein response to some degree.

Discussion

Hepatic steatosis and iron overload are not only pathophysiological features of HCV-associated chronic liver disease (5, 26) but also risk factors for the development of HCC (27, 28). The present animal model, FL-N/35 transgenic mice fed an excess iron diet, had several similarities with patients having HCV-associated chronic liver disease in terms of development of hepatic steatosis, followed by hepatocarcinogenesis (8), even though hepatic steatosis in this model was different from one observed in patients with HCV genotype 3 infection as to whether it was virally induced. In addition, the hepatic

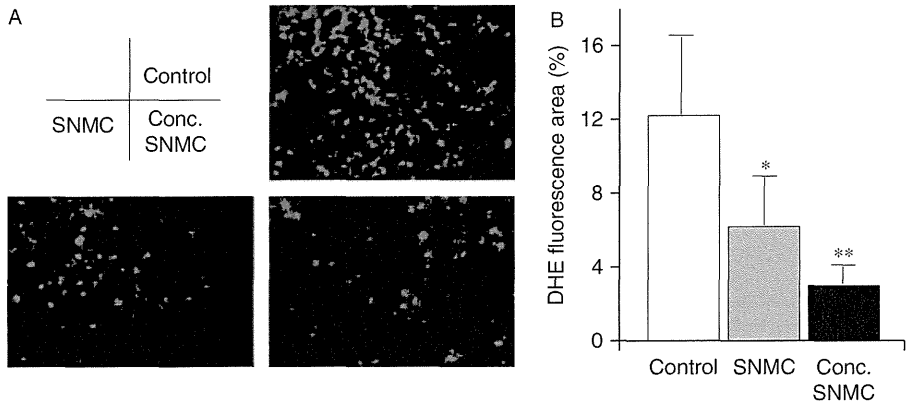

Fig. 5. Reactive oxygen species production in the liver in iron-overloaded FL-N/35 transgenic mice in each group. (A) Frozen liver sections of mice in each group were stained with dihydroethidium. (B) Fluorescence intensity was quantified by NIH image analysis software for three randomly selected areas of digital images for four mice in each group. Control, Stronger Neo-Minophagen C^{TM} (SNMC) and Conc. SNMC; see legend for Figure 1. $^{*}P < 0.005$ vs control, $^{**}P < 0.001$ vs control, $P < 0.05$ vs SNMC.

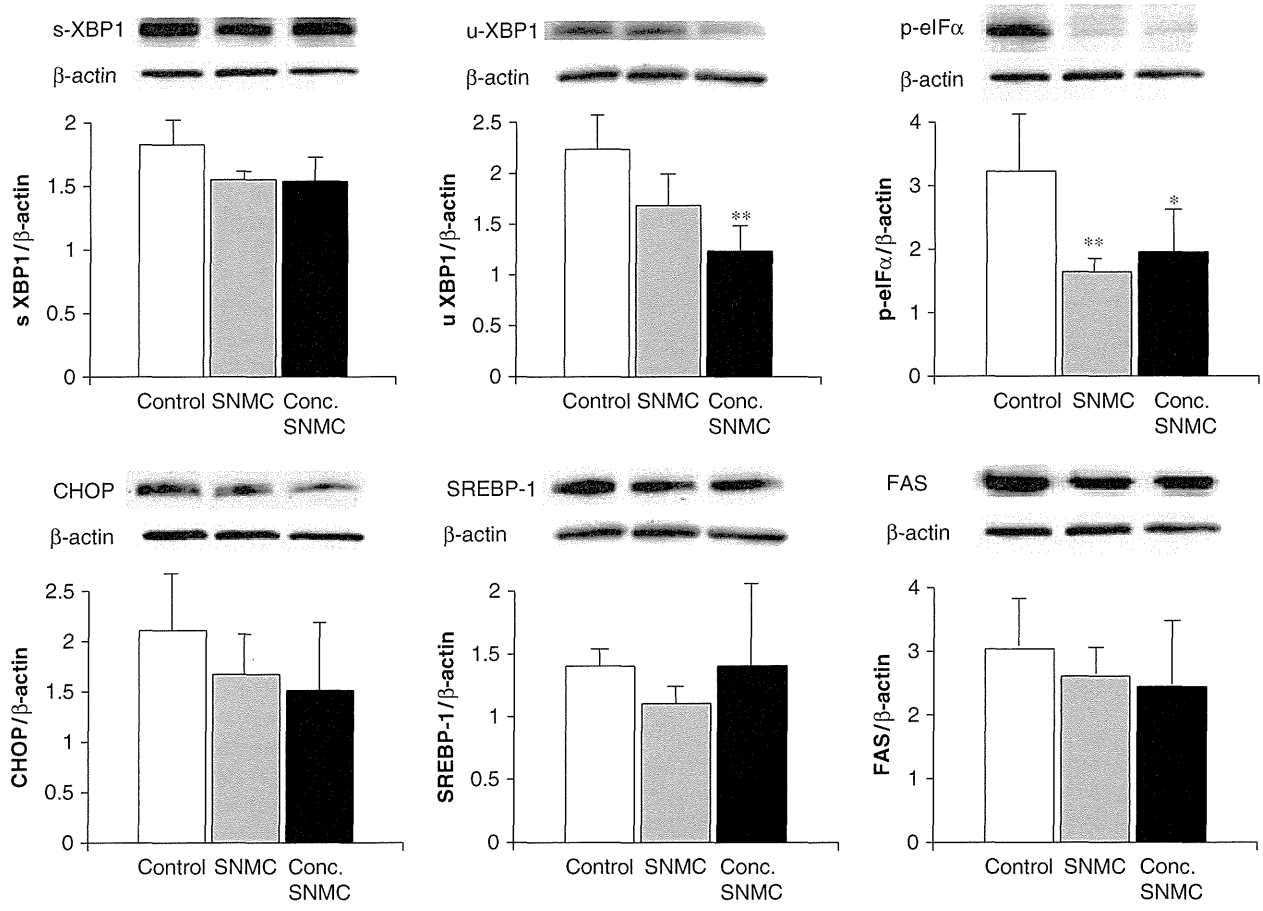

Fig. 6. Expression of spliced X-box DNA-binding protein 1 (sXBP-1), unspliced X-box DNA-binding protein 1 (uXBP-1), phosphorylated initiation factor-2α (p-IF2α), CCAAT/enhancer-binding protein homology protein (CHOP), sterol regulatory element-binding protein 1 (SREBP1) and fatty acid synthetase (FAS) in the liver in mice in each group. Immunoblots were performed using liver lysates from four mice in each group. The degree of protein expression was normalized with β-actin. Control, Stronger Neo-Minophagen C^{TM} (SNMC) and Conc. SNMC; see legend for Figure 1. $^{*}P < 0.05$ vs control, $^{**}P < 0.01$ vs control, $P < 0.05$ vs SNMC.

iron concentration of FL-N/35 transgenic mice fed the excess iron diet was comparable with that of a large number of patients with chronic hepatitis C in extensive studies (29, 30). Thus, FL-N/35 transgenic mice fed the excess iron diet appeared to be a suitable animal model to assess the effect of the long-term treatment with SNMC on the development of hepatic steatosis in HCV infection. The dose of SNMC administered to the FL-N/35 transgenic mice was comparable with the dosage given to patients with chronic hepatitis (approximately 100 ml of SNMC). This implies that a clinical dosage of SNMC has the potential to reduce hepatic steatosis occurring in patients with HCV-associated chronic liver diseases. There was no histological improvement such as inflammation or fibrosis regardless of serum ALT reduction in the human study, where the change of hepatic steatosis was not assessed (3). We could not evaluate whether SNMC has a potential to reduce inflammation or fibrosis in this study, because the present animal model did not show inflammation or fibrosis. Therefore, the decreased serum ALT levels in this model were thought to reflect the reduction of hepatic steatosis by SNMC.

Our previous study indicated that iron overload reinforced hepatic steatosis through ROS-induced activation of the unfolded protein response in FL-N/35 transgenic mice, and that an anti-oxidant, *N*-acetyl cysteine (NAC), almost completely blocked ROS production and cancelled hepatic steatosis induced by HCV proteins and iron (16). In the present study, SNMC reduced ROS production to a lesser degree than NAC. SNMC did not affect the hepatic iron content or hepcidin expression level, even though we reported previously the ROS-associated inhibition of hepcidin transcription in FL-N/35 transgenic mice (14). Nor did SNMC fully inhibit the ROS-associated unfolded protein response; nevertheless, SNMC effectively inhibited the development of hepatic steatosis in a dose-dependent manner through improvement of the mitochondrial structure, β-oxidation activity and CPTI expression. It should be noted that SNMC had a protective effect against mitochondrial injury rather than a simple anti-oxidative effect in FL-N/35 transgenic mice fed the excess iron.

Carnitine palmitoyl transferase I is negatively regulated by malonyl-CoA, an intermediate product in fatty acid synthesis, at the transcriptional level (18). Therefore, we need to consider at least two explanations for the increased CPTI expression induced by the 6-month treatment with SNMC. HCV core protein has been shown to be located on the mitochondrial outer membrane (19, 31), which may damage the membrane. One explanation is that SNMC increases CPTI expression through the restoration of the damaged mitochondrial outer membrane, as shown by the attenuated ultrastructural alterations of mitochondria with SNMC in FL-N/35 transgenic mice fed the excess iron. Another explanation is that SNMC may increase CPTI expression through the inhibition of fatty acid synthesis. However, the latter explanation seems unlikely, because the 6-month treatment with SNMC did not change the expression of SREBP1 or FAS (Fig. 6). Thus, the mechanisms by which SNMC reduces hepatic steatosis induced by HCV protein and iron overload may be mainly because of increased β-oxidation activity associated with increased CPTI stability through the protective effect against mitochondrial injury.

Of particular concern is how SNMC exerts its protective effect against mitochondrial injury. We reported previously that SNMC restored depletion of reduced glutathione (GSH) induced by CCl_4 and increased the synthesis of γ-glutamylcysteine synthetase (γ-GCS), a rate-limiting enzyme regulating GSH synthesis, at the transcriptional level in FL-N/35 transgenic mice (9). Judging from the protective effect of SNMC against mitochondrial injury, SNMC may play a role in the reduction of mitochondrial oxidative stress. Hepatic GSH synthesis is mainly regulated by the availability of cysteine, the sulphur amino acid precursor and the activity of γ-GCS. SNMC consists of 0.2 glycyrrhizin, 0.1 cycteine and 2.0% glycine in physiological solution. The cysteine included in SNMC may also contribute to GSH synthesis through its increased availability. The present study was largely observational and therefore further analysis is needed to clarify the mechanisms by which SNMC exerts a protective effect against mitochondrial injury.

In conclusion, this study shows that SNMC reduces hepatic steatosis induced by HCV protein and iron overload in mice by inducing increased β-oxidation activity associated with an increased CPTI expression.

Acknowledgements

This study was supported by a grant from the Ministry of Education, Culture, Sports, Science and Technology (No. 20590782), and in part by a Research on Hepatitis, Health and Labour Sciences Research Grants from the Ministry of Health, Labor and Welfare, Japan.

References

1. Seeff LB. Natural history of chronic hepatitis C. *Hepatology* 2002; **36**: S35–46.
2. Fried MW, Shiffman ML, Reddy KR, *et al.* Peginterferon alfa-2a plus ribavirin for chronic hepatitis C virus infection. *N Engl J Med* 2002; **347**: 975–82.
3. Orlent H, Hansen BE, Willems M, *et al.* Biochemical and histological effects of 26 weeks of glycyrrhizin treatment in chronic hepatitis C: a randomized phase II trial. *J Hepatol* 2006; **45**: 539–46.
4. Arase Y, Ikeda K, Murashima N, *et al.* The long term efficacy of glycyrrhizin in chronic hepatitis C patients. *Cancer* 1997; **79**: 1494–500.
5. Farinati F, Cardin R, De Maria N, *et al.* Iron storage, lipid peroxidation and glutathione turnover in chronic anti-HCV positive hepatitis. *J Hepatol* 1995; **22**: 449–56.

6. Kitase A, Hino K, Furutani T, *et al.* In situ detection of oxidized n-3 polyunsaturated fatty acids in chronic hepatitis C: correlation with hepatic steatosis. *J Gastroenterol* 2005; **40**: 617–24.
7. Barbaro G, Di Lorenzo G, Asti A, *et al.* Hepatocellular mitochondrial alterations in patients with chronic hepatitis C: ultrastructural and biochemical findings. *Am J Gastroenterol* 1999; **94**: 2198–205.
8. Furutani T, Hino K, Okuda M, *et al.* Hepatic iron overload induces hepatocellular carcinoma in transgenic mice expressing the hepatitis C virus polyprotein. *Gastroenterology* 2006; **130**: 2087–98.
9. Hidaka I, Hino K, Korenaga M, *et al.* Stronger Neo-Minophagen C^{TM}, a glycyrrhizin-containing preparation, protects liver against carbon tetrachloride-induced oxidative stress in transgenic mice expressing the hepatitis C virus polyprotein. *Liver Int* 2007; **27**: 845–53.
10. Beard MR, Abell G, Honda M, *et al.* An infectious molecular clone of a Japanese genotype 1b hepatitis C virus. *Hepatology* 1999; **30**: 316–24.
11. Lerat H, Honda M, Beard MR, *et al.* Steatosis and liver cancer in transgenic mice expressing the structural and nonstructural proteins of hepatitis C virus. *Gastroenterology* 2002; **122**: 352–65.
12. Bligh EG, Dyer WJ. A rapid method of total lipid extraction and purification. *Can J Biochem Physiol* 1959; **37**: 911–7.
13. Lowry OH, Rosebrough NJ, Farr AL, Randall RJ. Protein measurement with the Folin phenol reagent. *J Biol Chem* 1951; **193**: 265–75.
14. Nishina S, Hino K, Korenaga M, *et al.* Hepatitis C virus-induced reactive oxygen species raise hepatic iron level in mice by reducing hepcidin transcription. *Gastroenterology* 2008; **134**: 226–38.
15. Harrison-Findik DD, Schafer D, Klein E, *et al.* Alcohol metabolism-mediated oxidative stress down-regulates hepcidin transcription and leads to increased duodenal iron transporter expression. *J Biol Chem* 2006; **281**: 22974–82.
16. Nishina S, Korenaga M, Hino K, *et al.* Hepatitis C virus protein and iron overload induce hepatic steatosis through the unfolded protein response in mice. *Liver Int* 2010; **30**: 683–92.
17. Rao MS, Reddy JK. Peroxisomal beta-oxidation and steatohepatitis. *Semin Liver Dis* 2001; **21**: 43–55.
18. Kerner J, Hoppel C. Fatty acid import into mitochondria. *Biochim Biophys Acta* 2000; **1486**: 1–17.
19. Korenaga M, Wang T, Li Y, *et al.* Hepatitis C virus core protein inhibits mitochondrial electron transport and increases reactive oxygen species (ROS) production. *J Biol Chem* 2005; **280**: 37481–8.
20. Horton JD, Goldstein JL, Brown MS. SREBPs: activators of the complete program of cholesterol and fatty acid synthesis in the liver. *J Clin Invest* 2002; **109**: 1125–31.
21. Ji C, Kaplowitz N. ER stress: can the liver cope? *J Hepatol* 2006; **45**: 321–33.
22. Calfon M, Zeng H, Urano F, *et al.* IRE1 couples endoplasmic reticulum load to secretory capacity by processing the XBP-1 mRNA. *Nature* 2002; **415**: 92–6.
23. Yoshida H, Matsui T, Yamamoto A, Okada T, Mori K. XBP1 mRNA is induced by ATF6 and spliced by IRE1 in response to ER stress to produce a highly active transcription factor. *Cell* 2001; **107**: 881–91.
24. Marciniak SJ, Ron D. Endoplasmic reticulum stress signaling in disease. *Physiol Rev* 2006; **86**: 1133–49.
25. Okada T, Yoshida H, Akazawa R, Negishi M, Mori K. Distinct roles of activating transcription factor 6 (ATF6) and double-stranded RNA-activated protein kinase-like endoplasmic reticulum kinase (PERK) in transcription during the mammalian unfolded protein response. *Biochem J* 2002; **366**: 585–94.
26. Scheuer PJ, Ashrafzadeh P, Sherlock S, Brown D, Dusheiko GM. The pathology of hepatitis C. *Hepatology* 1992; **15**: 567–71.
27. Ohata K, Hamasaki K, Toriyama K, *et al.* Hepatic steatosis is a risk factor for hepatocellular carcinoma in patients with chronic hepatitis C virus infection. *Cancer* 2003; **97**: 3036–43.
28. Kato J, Kobune M, Nakamura T, *et al.* Normalization of elevated hepatic 8-hydroxy-2′-deoxyguanosine levels in chronic hepatitis C patients by phlebotomy and low iron diet. *Cancer Res* 2001; **61**: 8697–702.
29. Hofer H, Osterreicher C, Jessner W, *et al.* Hepatic iron concentration does not predict response to standard and pegylated-IFN/ribavirin therapy in patients with chronic hepatitis C. *J Hepatol* 2004; **40**: 1018–22.
30. Rulyak SJ, Eng SC, Patel K, *et al.* Relationships between hepatic iron content and virologic response in chronic hepatitis C patients treated with interferon and ribavirin. *Am J Gastroenterol* 2005; **100**: 332–7.
31. Schwer B, Ren S, Pietschmann T, *et al.* Targeting of hepatitis C virus core protein to mitochondria through a novel C-terminal localization motif. *J Virol* 2004; **78**: 7958–68.

Journal of Gastroenterology and Hepatology

A novel des-γ-carboxy prothrombin in serum for the diagnosis of hepatocellular carcinoma.

Journal:	*Journal of Gastroenterology and Hepatology*
Manuscript ID:	JGH-01249-2012.R1
Manuscript Type:	Original Article - Hepatology (Clinical)
Date Submitted by the Author:	n/a
Complete List of Authors:	Tanaka, Takahiro; Institutes of Health Biosciences, University of Tokushima Graduate School, Department of Gastroenterology and Oncology Taniguchi, Tatsuya; Institutes of Health Biosciences, University of Tokushima Graduate School, Department of Gastroenterology and Oncology Sannomiya, Katsutaka; Institutes of Health Biosciences, University of Tokushima Graduate School, Department of Gastroenterology and Oncology Takenaka, Hidetaka; Institutes of Health Biosciences, University of Tokushima Graduate School, Department of Gastroenterology and Oncology Tomonari, Tetsu; Institutes of Health Biosciences, University of Tokushima Graduate School, Department of Gastroenterology and Oncology Okamoto, Koichi; Institutes of Health Biosciences, University of Tokushima Graduate School, Department of Gastroenterology and Oncology Kitamura, Shinji; Institutes of Health Biosciences, University of Tokushima Graduate School, Department of Gastroenterology and Oncology Okahisa, Toshiya; Institutes of Health Biosciences, University of Tokushima Graduate School, Department of Gastroenterology and Oncology Tamaki, Katsuyoshi; Institutes of Health Biosciences, University of Tokushima Graduate School, Department of Gastroenterology and Oncology Mikasa, Hiroaki; Faculty of Medicine, Tokushima University, Medical Education Support Center Suzuki, Sadao; Nagoya City University Graduate School of Medical Sciences, Department of Public Health Takayama, Tetsuji; Institutes of Health Biosciences, University of Tokushima Graduate School, Department of Gastroenterology and Oncology
Key Words:	Hepatocellular carcinoma, clinical < Hepatology, Cell and molecular biology < Hepatology, Hepatocellar carcinoma, treatment < Hepatology

A novel des-γ-carboxy prothrombin in serum for the diagnosis of hepatocellular carcinoma.

A short running title: Novel DCP for diagnosis of HCC

Takahiro Tanaka,* Tatsuya Taniguchi,* Katsutaka Sannomiya,* Hidetaka Takenaka,* Tetsu Tomonari,* Koichi Okamoto,* Shinji Kitamura,* Toshiya Okahisa,* Katsuyoshi Tamaki,* Hiroaki Mikasa, † Sadao Suzuki‡ and Tetsuji Takayama*

* Department of Gastroenterology and Oncology, Institutes of Health Biosciences, University of Tokushima Graduate School, 3-18-15, Kuramoto-cho, Tokushima 770-8503, Japan.
†Medical Education Support Center, Faculty of Medicine, Tokushima University.
‡Department of Public Health, Nagoya City University Graduate School of Medical Sciences, Nagoya 467-8601, Japan.

Corresponding author: Tetsuji Takayama, MD, PhD, Department of Gastroenterology and Oncology, Institute of Health Biosciences, University of Tokushima Graduate School, 3-18-15, Kuramoto-cho, Tokushima 770-8503, Japan.
E-mail; takayama@clin.med.tokushima-u.ac.jp
TEL; +81-88-633-7122, FAX; +81-88-633-9235

number of table, 1; number of figures, 5.

Abstract

Background and Aim: We meassured serum des-γ-carboxy prothrombin (DCP) levels using a newly developed electrochemiluminescence immunoassay (ECLIA, NX-DCP) and investigated the utility of NX-DCP and DCP/NX-DCP ratio for the diagnosis of hepatocellular carcinoma (HCC). We also elucidated antigenic differences in DCP between HCC and non-HCC patients.

Methods: The subjects included 170 patients with HCC, 61 with benign liver disease, 12 with obstructive jaundice, and 10 warfarin users. NX-DCP was quantitated by sandwich ECLIA employing novel anti-DCP monoclonal antibodies, P11 and P16. Conventional DCP was quantitated by standard ECLIA. DCP extracted from serum by affinity-chromatography was analyzed by western blotting.

Results: Conventional serum DCP levels were high in patients with HCC and obstructive jaundice and in warfarin users, consistent with previous reports. Serum NX-DCP levels were high only in warfarin users and obstructive jaundice patients (vitamin K-defficient patients), but not in HCC patients. The DCP/NX-DCP ratio was significantly higher in the HCC group than in the benign liver disease, obstructive jaundice, and warfarin groups ($P<0.001$). Receiver-operating characteristic analysis showed significant superiority of the DCP/NX-DCP ratio over conventional DCP as a marker for HCC diagnosis ($P<0.05$). Western blot analysis showed that P11 and P16 reacted strongly with DCP from a warfarin user and an obstructive jaundice patient, but very faintly with DCP from an HCC patient. Immunohistochemistry on HCC samples and autopsied normal liver tissues from warfarin users showed similar results.

Conclusions: The DCP/NX-DCP ratio is very useful for diagnosing HCC. DCP in HCC patients is distinct from that in vitamin K-deficient patients.

Keywords: des-γ-carboxyl prothrombin, hepatocellular carcinoma, warfarin, obstructive jaundice.

Introduction

Hepatocellular carcinoma (HCC) is the sixth most common tumor type and the third most common cause of cancer-related death worldwide.[1] It is well recognized that serological markers including α-fetoprotein (AFP) and des-γ-carboxy prothrombin (DCP) are very important for the diagnosis of HCC, as are imaging modalities such as computed tomography (CT) and ultrasound.

DCP is a well-known tumor marker for diagnosis, screening, and therapeutic monitoring of HCC.[2-6] It has been reported that DCP has a sensitivity of 39% to 81% and specificity of 68% to 97% for the detection of HCC.[2,5-9] In comparison, DCP has sensitiity similar to that of AFP but is more specific. Moreover, tumor recurrence and metastasis are more frequent in HCC patients who are DCP positive than in HCC patients who are DCP negative, indicating that DCP is a prognostic factor for HCC.[4,10,11] It has also been reported that DCP is an autologous growth factor for HCC, binding directly to the hepatocyte growth factor receptor (c-MET), and that DCP promotes vascular endothelial cell proliferation and migration.[12,13] In this context, DCP is a very useful marker for prognostic prediction as well as for diagnosis and surveillance of HCC.

DCP is an aberrant prothrombin that lacks the ability to interact with other coagulation factors. The prothrombin molecule has 10 γ-carboxylated glutamic acid (Gla) residues in the Gla domain of the N-terminal region. All of the 10 glutamic acid (Glu) residues in prothrombin precursor need to be γ-carboxylated by the vitamin K-dependent enzymatic reaction of γ-glutamylcarboxylase through post-translational modification.[14] DCP is an incomplete prothrombin in which some Glu residues do not undergo γ-carboxylation.[15] Therefore, in patients receiving warfarin, a vitamin K antagonist, serum DCP levels are abnormally high.[16,17] Similarly, in patients with obstructive jaundice or jaundice due to liver failure, the serum DCP often shows abnormally high levels due to a lack of vitamin K even in the absence of HCC.[18] Thus, the major drawback of DCP as a tumor marker is that it cannot be used to determine the diagnosis and prognosis of HCC in these patients. Likewise, serum DCP levels do not reflect the tumor size in patients with HCC and concomitant jaundice.

Currently, the most commonly used kit for measuring serum DCP concentrations is the picolumi PIVKA-II (EIDIA Co., Ltd, Tokyo, Japan), in which anti-DCP monoclonal antibody MU-3 recognizing acarboxy 19,20-Glu DCP and rabbit anti-human prothrombin polyclonal antibody are used.[11,19,20] Studies on DCP heterogeneity in HCC patients suggest that the number of Gla residues in DCP can vary.[16,21] However, to our knowledge, differences in DCP between HCC patients and vitamin K-deficient patients have been analyzed in only one study, by Uehara and colleagues.[16] In that study, an analysis of DCP carboxylation status in a single warfarin user, none of the Glu residues were carboxylated. Recently, Toyoda and associates measured a novel DCP (NX-DCP) in serum using a newly developed sandwich ECLIA with new anti-DCP monoclonal antibodies p11 and p16 and reported preliminary data from only 20 HCC patients.[22] They showed that the DCP/NX-DCP ratio may be useful for the diagnosis of HCC among warfarin users. However, no studies to date have assessed NX-DCP in a large number of HCC patients, nor has NX-DCP been compared among HCC, liver cirrhosis (LC)/chronic hepatitis (CH), obstructive jaundice, and warfarin-treated patients. Therefore, in this study, we prospectively evaluated the serum NX-DCP level and DCP/NX-DCP ratio using a novel ECLIA method in patients with HCC, LC/CH, or obstructive jaundice, and in warfarin users for the diagnosis of HCC. We also analyzed the reactivity of DCP to P11, P16, and MU-3 to identify structural differences in DCP from HCC patients and patients with vitamin K deficiency due to obstructive jaundice and warfarin use.

Methods

Patients. This study was approved by the institutional review board of Tokushima University Hospital, Tokushima, Japan. During the period from April 2010 to August 2012, a total of 176 patients with HCC, 13 patients with LC, 48 patients with CH, 12 patients with obstructive jaundice (total bilirubin ≥ 5.0 mg/dl) due to advanced gastrointestinal cancer (ie, gastric cancer, pancreatic cancer), and 10 patients receiving warfarin for cardiac diseases were prospectively enrolled after obtaining written informed consent. HCC was diagnosed based on the following

classic imaging manifestations: (i) early enhancement at the arterial phase and hypoattenuation at the portal venous phase or at the equilibrium phase on contrast-enhanced dynamic CT; and (ii) hyperattenuation on CT during hepatic arteriography and hypoattenuation on CT during arterialportography.[23,24] The WHO clasification of HCC was used for HCC staging. A 2-mL blood sample was drawn from each patient for validation of the new ECLIA method for measuring serum DCP concentrations. Furthermore, additional 10-mL blood samples were drawn from 3 of the patients (a patient with HCC, a warfarin user, and an obstructive jaundice patient) for western blot analysis of DCP. All the blood samples were centrifuged to obtain serum. Lastly, 3 HCC tissue samples were obtained surgically from patients with HCC and 2 normal liver tissue samples were obtained at autopsy from 2 patients who had received warfarin. These tissues were used for immunohistochemical analysis of DCP.

NX-DCP and DCP quantitation by sandwich ECLIA. The serum NX-DCP concentration was measured using a new sandwich ECLIA method (kindly provided by EIDIA Co, Ltd., Tokyo, Japan). The method employs the novel mouse anti-human DCP monoclonal antibodies p11 and p16 which were generated by immunization with DCP from a warfarin user (Sekisui Medical Co., Ltd. Tokyo, Japan). The conventional serum DCP concentration was measured using the picolumi PIVKA-II (cutoff value 40 mAU/ml) method.[19] The method employed mouse anti-human DCP antibody MU-3 and rabbit anti-human prothrombin polyclonal antibody.[20]

Affinity chromatography of DCP. All steps were performed at 4°C. DCP and prothrombin were separated on a Sepharose 4B column coupled with mouse anti-human prothrombin F2 monoclonal antibody, and the column was then washed with Tris-buffered saline (TBS, pH=7.8). Bound protein was eluted with 2 M guanidine-HCl then immediately pooled and dialyzed in TBS.

Western blot analysis. The purified protein and prothrombin (Abcam plc, Cambridge, UK) as a control were separated by SDS-PAGE and transferred to a polyvinylidene difluoride membrane.